Research Square

Preprints are preliminary reports that have not undergone peer review.
They should not be considered conclusive, used to inform clinical practice,
or referenced by the media as validated information.

Identification of prognostic markers related to triaptosis in endometrial cancer and construction of prognostic model

Nanqing Zhou
Affiliated Hospital of Guizhou Medical University
Lihua Yang
Affiliated Hospital of Guizhou Medical University
Jie Ren
Affiliated Hospital of Guizhou Medical University
WenChi Xu
605338101@qq.com

Guizhou Provincial People's Hospital
Jin Li
Affiliated Hospital of Guizhou Medical University
Xu Zhang
Affiliated Hospital of Guizhou Medical University
Zirui Wu
Affiliated Hospital of Guizhou Medical University
HeWei Shi
Affiliated Hospital of Guizhou Medical University
Fumei Zhang
Affiliated Hospital of Guizhou Medical University
Qin Tian
Affiliated Hospital of Guizhou Medical University
Changya Li
Affiliated Hospital of Guizhou Medical University
Lu Xiong
The First Affiliated Hospital of Sun Yat-sen University, Guizhou Hospital
WanLi Chen
Affiliated Hospital of Guizhou Medical University
Ting Guo
Affiliated Hospital of Guizhou Medical University
Pei Huang

Guiyang Fourth People's Hospital

Min Xiao

Guiyang Huaxi District Hospital of Traditional Chinese Medicine

YunChuan Jia

Guiyang Huaxi District Hospital of Traditional Chinese Medicine

Jing Wang

Affiliated Hospital of Guizhou Medical University

Article

Keywords: Endometrial cancer, Triaptosis, Prognostic markers, Immune infiltration

Posted Date: November 11th, 2026

DOI: https://doi.org/10.21203/rs.3.rs-11282398/v1

License: This work is licensed under a Creative Commons Attribution 4.0 International License.
Read Full License

Additional Declarations: No competing interests reported.

Abstract

Background

Endometrial cancer (EC) is a malignant neoplasm of the uterine epithelial lining. Triaptosis is a kind of cell death induced by endosomal dysfunction due to PI3P depletion. Triaptosis is suggested to correlate with EC, but the mechanism remains unclear. We aimed to identify triaptosis-related prognostic markers in EC and reveal their mechanisms via bioinformatics..

Methods

Weighted correlation network analysis (WGCNA) screened triaptosis related genes (TRGs) in TCGA-UCEC, defined as WGCNA-TRGs. Candidate genes (CGs) were derived by intersecting WGCNA-TRGs with differentially expressed genes (DEGs) extracted from the TCGA-UCEC. Prognostic markers were screened through univariate Cox proportional hazards model and LASSO regression. Prognostic model was constructed and validated in TCGA-UCEC and validation set. A nomogram estimated independent prognostic factors. Immune infiltration and gene set enrichment analysis (GSEA) profiled tumor-infiltrating immune cells and related pathways..

Results

There were 110 CGs were identified and 4 prognostic markers (SDF2L1, STK26, TDRKH and USP18) were determined. Prognostic model performed well in TCGA-UCEC and validation set. Both tumor stage and risk score were validated as independent prognostic determinants, with the nomogram built upon these two factors yielding robust predictive accuracy for patient prognosis. Among immune cell subsets, several populations—most notably activated B cells—exhibited substantial abundance differences across the high- and low-risk strata. There were common 12 pathways shared by prognostic markers. Drugs like ZINC were commonly shared by prognostic markers.

Conclusion

SDF2L1, STK26, TDRKH, and USP18 were characterized as triaptosis-associated prognostic markers in EC, offering a theoretical foundation for the development of targeted therapies.

1. Introduction

Endometrial cancer (EC), arising from the malignant transformation of the uterine epithelial lining, typically presents with abnormal uterine bleeding; endometrial hyperplasia is widely regarded as its precancerous lesion. It is associated with reproductive endocrine disorders, excessive estrogen stimulation, early menarche, late menopause, and infertility[1]. EC typically arises under conditions of

prolonged estrogen dominance, where estrogen induces mitogenic stimulation, ultimately leading to malignant transformation of endometrial glandular epithelium[2]. Key risk factors include advanced age, obesity, hypertension, and diabetes[3]. Visceral fat secretes adipokines that promote endometrial hyperplasia and tumorigenesis, and adipose tissue serves as a source of mesenchymal stem cells supporting tumor growth and progression[4], as well as the primary site of postmenopausal estrogen synthesis via aromatase-mediated conversion of androgens to estrogen, underscoring the strong link between obesity and EC[5]. Metabolic alterations in EC include aberrant cholesterol uptake and increased fatty acid synthesis[6]. Additionally, changes in microbiota composition, immune cell profiles, and inflammatory gene expression patterns significantly influence EC progression[7]. Estrogen modulates the female reproductive microenvironment by enhancing Lactobacillus abundance and lactate production[8] and may promote inflammation[9], while chronic inflammation, through free radical formation, elevates DNA damage risk and correlates with endometrial cell proliferation[10]. Glycosylation modifications of endometrial cell surface proteins, such as N-linked glycoproteins, regulate cell proliferation and apoptosis in EC[11], whereas in healthy tissues, glycosylation facilitates embryo positioning and trophoblast adhesion and invasion for successful implantation[12]. The heterogeneity of EC histological subtypes and molecular phenotypes influences surgical and adjuvant therapy choices[13], necessitating further research into pathogenesis and novel molecular targets to refine classification and enable more efficient, personalized treatment.

Triaptosis, a recently identified cell death mechanism, is closely linked to endosomal dysfunction and adverse cellular responses induced by oxidative stress. This pathway involves the inhibition of phosphatidylinositol 3-kinase VPS34 (PIK3C3/VPS34) by oxidative stress, leading to depletion of phosphatidylinositol triphosphate (PI3P)—a key lipid product catalyzed by VPS34—and ultimately resulting in cell death[14]. As a lipid kinase, VPS34 functions as a key regulatory node linking autophagy to glycolysis via lactylation, thereby facilitating both autophagy flux and endolysosomal transport[15]. Furthermore, VPS34 occupies a pivotal position in endosome-lysosome vesicle trafficking: PI3P generated by its kinase activity directs the fate of derived vesicles, either routing them back to the plasma membrane through recycling pathways or channeling them into the lysosomal degradation system[16]. In the context of endometrial physiology and pathology, autophagy and cell death are key players in various processes, such as eliminating senescent endometrial cells during the secretory and menstrual phases[17] and facilitating endometrial stromal cell differentiation into epithelioid cells to support pregnancy[18]. In EC progression, dysregulation of these pathways is evident; for instance, overexpression of estrogen-related receptor α promotes glycolysis to limit pyroptosis, thereby enhancing EC invasion and metastasis[19], while active components from lotus seeds induce mitochondrial apoptosis and endoplasmic reticulum stress to trigger EC cell death[20]. Although research on Triaptosis remains limited, existing evidence suggests its relevance: niclosamide treats EC by inducing autophagy and lysosome-dependent cell death[21], and oxidative stress with ROS accumulation promotes pyroptosis to inhibit EC growth[22]. Oxidative stress and the endosomal system are key aspects of inositol trisphosphate-mediated apoptosis, suggesting a link to EC and potentially serving as important targets for limiting EC progression.

An integrated multi-omics analytical framework was applied to systematically uncover triaptosis-related prognostic biomarkers in EC along with their underlying molecular regulatory mechanisms. Drawing on transcriptomic data from EC patients available in the TCGA database, candidate prognostic biomarkers were filtered through univariate Cox regression analysis and Least Absolute Shrinkage and Selection Operator (LASSO) regression analysis. Furthermore, bioinformatics methods were applied to comprehensively analyze the biological characteristics and functional mechanisms of these biomarkers from multiple dimensions, including functional enrichment, immune microenvironment regulation, and molecular interaction networks. Additionally, through targeted drug screening, this study evaluated the potential therapeutic value of the prognostic biomarkers, providing new targets and theoretical support for the clinical treatment of EC.

2. Materials and methods

2.1 Data source

The TCGA-UCEC dataset was downloaded from The Cancer Genome Atlas Program (TCGA) public repository (http://cancergenome.nih.gov/), encompassing tissue specimens from 550 EC patients alongside 35 matched samples collected from healthy controls. We further divided the 546 samples with survival information by 3:7 ratio and took the 30% (383 samples) as validation set for prognostic model validation. In addition, 21 triaptosis related genes (TRGs) were obtained from previous researches[23] (Table S1) .

2.2 Weighted correlation network analysis (WGCNA)

Gene set variation analysis (GSVA) scores for TRGs were computed using the GSVA package (v 1.50.0) [24], enabling quantitative comparison between EC and control groups within the TCGA-UCEC cohort at a significance threshold of $P < 0.05$; the resulting data were subsequently visualized with the ggplot2 package (v 3.5.2)[25]. Subsequently, we conducted WGCNA analysis to obtain the related modules of TRGs, using WGCNA package (v 1.7.1)[26]. First, we clustered the samples by Hclust function to remove those outliers. Based on topology model and mean connectivity of WGCNA, we selected the best power to construct scale-independence network by PickSoftThreshold function, scale-independent R2 value (R2) > 0.85 and mean connectivity < 200. Modules were divided by blockwiseModules with minModuleSize = 100. Next, we calculated the correlation coefficients (cor) and P value of modules and TRGs scores, and selected key modules with cor > 0.3 and pvalue < 0.05. Genes assigned to the key modules identified by WGCNA were collectively designated as WGCNA-TRGs.

2.3 Screening of differentially expressed genes (DEGs) and candidate genes (CGs)

DEGs between EC patient samples and healthy controls were screened from the TCGA-UCEC dataset via the DESeq2 package (v. 1.42.2)[27], applying thresholds of $|\log_2 FC| > 1.5$ and adjusted (adj.) P value < 0.05. The top 10 upregulated and downregulated genes, ranked by ascending $\log_2 FC$, were displayed in a

heatmap generated with ComplexHeatmap (v. 2.18.0)[28] and a volcano plot rendered with ggplot2 (v. 3.5.2). The overlap between WGCNA-TRGs and DEGs was subsequently determined using the VennDiagram package (v. 1.7.3)[29], and the resulting intersection constituted the CGs for downstream analyses.

2.4 Function enrichment analysis and acquisition of key CGs

To delineate the potential biological functions of the CGs, Gene Ontology (GO) and Kyoto Encyclopedia of Genes and Genomes (KEGG) enrichment analyses were carried out using ClusterProfiler (v. 4.10.1)[30] at a significance threshold of $P < 0.05$. The GO analysis encompassed three principal categories: biological process (BP), cellular component (CC), and molecular function (MF). The top five enriched GO terms and KEGG pathways were ranked by ascending P value for visualization. PPI Networks among the CGs were additionally retrieved from the STRING database (www.string-db.org), retaining only interactions with a confidence score exceeding 0.4.

2.5 Screening prognostic markers

Candidate prognostic markers among the key CGs were filtered by univariate Cox analysis ($P < 0.05$, $HR \neq 1$) combined with a PH assumption test ($P > 0.05$), both implemented via the survival package (v. 3.7.0) [31]. The resulting Cox analysis outputs were presented as forest plots generated by the forestplot package (v. 3.1.3)[32].

The LASSO regression model were conducted through ten-fold cross-validation and confirmed the prognostic markers with coefficient ≠ 0, based on minimum lambda value (lambda.min), using glmnet package (v. 4.1.4)[33].

2.6 Prognostic model construction and validation

Based on the LASSO coefficient (Table S2), we calculated the risk score of each patient in TCGA-UCEC and validation set by (i represented each sample) : Risk score = ∑i Coefficient (LASSO)*Expression of gene(i)

An optimal cutoff was applied to stratify patients from the TCGA-UCEC cohort and the external validation set into high- and low-risk categories. Inter-group survival disparities were then quantified through K-M survival analysis ($P < 0.05$) via the survival package (v. 3.7.0), and the discriminatory capacity of the risk score was further assessed by ROC curves for 3-, 5-, and 7-year overall survival generated with the survivalROC package (v 1.0.3)[34], where area under curve (AUC) > 0.6 was taken as the criterion for adequate discrimination.

2.7 Nomogram of prognostic markers

Age, race, tumor stage, and the TCGA-UCEC-derived risk score were collectively evaluated through univariate Cox regression ($P < 0.05$, $HR \neq 1$) and a PH assumption test ($P > 0.05$) using the survival

package (v. 3.7.0), with the aim of pinpointing clinically meaningful prognostic factors. Those meeting the screening criteria were subsequently incorporated into multivariate Cox regression ($P < 0.05$, $HR \neq 1$) alongside a PH test ($P > 0.05$) to confirm their status as independent prognostic contributors.

A nomogram incorporating the identified prognostic markers was developed with the rms package (v. 6.5.0)[35], drawing on the complete set of tissue samples available in the TCGA-UCEC dataset, so as to quantify their individual and combined predictive contributions. The nomogram assigned scores to each the independent prognostic factor. Aggregating individual item scores into a total point value allowed estimation of the 3-, 5-, and 7-year probability of EC occurrence. The regplot package (v. 1.1)[36] was further used to generate a calibration curve, enabling quantitative evaluation of how closely the model's predictions aligned with actual clinical observations. Decision curve analysis (DCA) alongside ROC curves (AUC > 0.7) were further applied to appraise the clinical net benefit and overall predictive performance of the nomogram.

2.8 Gene set enrichment analysis (GSEA)

The KEGG gene set "c2.cp.kegg.v7.5.1.symbols.gmt" downloaded from the Molecular Signatures Database (MSigDB)[37] served as the reference collection for examining pathway-level differences between risk groups. Differential expression profiling of the TCGA-UCEC cohort was performed using the DESeq2 package (v 1.40.2), and DEGs were ordered according to their log2FC values prior to GSEA. GSEA was then carried out through the ClusterProfiler package (v 4.10.1), retaining results with $|NES| > 1$ and $adj.P < 0.05$. The five leading pathways in each risk group were displayed in descending order of adj.P. The signaling pathways functionally linked to the prognostic markers were further characterized by Spearman correlation analysis performed with the psych package (v 2.4.3); genes ranked in descending order of their Spearman correlation coefficients were then subjected to GSEA, and the top five resultant pathways were visualized in descending order of adj.P using the enrichplot package (v 1.22.0)[38]. Finally, the common pathways shared by prognostic markers were revealed using ggvenn package (v 0.1.10)[39].

2.9 Immune infiltration analysis

Infiltration abundance scores across 28 immune cell types[40] were computed by single-sample gene set enrichment analysis (ssGSEA) and displayed as heatmaps through the pheatmap package (v 1.0.12)[40] enabling side-by-side comparison of immune landscapes between risk groups. Immune cell subsets exhibiting statistically significant differences between the high- and low-risk groups were then identified by Wilcoxon test ($P < 0.05$) and graphically presented using the ggplot2 package (v 3.5.2). Within the TCGA-UCEC dataset, pairwise Spearman correlation analysis—implemented via the psych package (v 2.4.3)[41]—was performed to quantify co-variation among differentially infiltrated immune cells and between each prognostic marker and those immune cell subsets, retaining associations with $|cor| > 0.3$ and $P < 0.05$.

Immune dysfunction and immune exclusion within the tumor microenvironment (TME) were evaluated using the Tumor Immune Dysfunction and Exclusion (TIDE) algorithm, with scores retrieved from the

TIDE database (http://tide.dfci.harvard.edu/). Differences in TIDE-derived metrics between the high- and low-risk groups were then compared at a significance threshold of $P < 0.05$.

2.10 Drug sensitivity analysis and drug target prediction

Per-patient median inhibitory concentration (IC50) values within the TCGA-UCEC cohort were predicted by feeding drug sensitivity data from the Genomics of Drug Sensitivity in Cancer (GDSC) database into the oncoPredict package (v 1.2)[42]. Between-group IC50 disparities were compared using the Wilcoxon rank-sum test ($P < 0.05$), with distributions illustrated through the ggplot2 package (v 3.5.2)[43]. Candidate therapeutic agents for EC were identified by querying the Drug Signatures database (DSigDB) [44] for compounds targeting the prognostic markers, with queries executed through the enrichR package (v 3.2)[45]. The interaction relationships between prognostic markers and candidate drugs were mapped into a network diagram using Cytoscape software (v 3.9.1)[46].

2.11 Statistical analysis

Statistical analyses throughout this study were carried out in R (v 4.3.1); between-group comparisons relied on the Wilcoxon test, with $P < 0.05$ serving as the threshold for statistical significance.

3. Results

3.1. Acquisition of 4,253 WGCNA-TRGs

TRG-based GSVA scores differed markedly between EC and control groups ($P < 0.001$) (Fig. 1A), and an optimal cutoff of 1.305393 enabled reliable stratification of samples into high- and low-risk groups ($P < 0.05$) (Fig. 1B). No outliers were detected, and a soft-thresholding power of 10 was selected as optimal (Fig. 1C, D). Two modules — brown and turquoise — were designated as key modules and collectively harbored 4,253 genes, which were defined as WGCNA-TRGs (Fig. 1E, F, Table S3, 4).

3.2 Acquisition of 110 CGs and functional enrichment analysis

A total of 3,442 DEGs between EC and control groups in TCGA-UCEC dataset were obtained. Among them, 2,039 genes, such as DKK4 and FGF3, were upregulated and 1,403 genes, such as PAEP and C7 were downregulated in EC samples compared with control samples (Figure.2A, B; Table S5). Subsequently, 110 CGs were obtained by taking the intersection of WGCNA-TRGs and DEGs (Figure.2C, Table S6) .

In GO enrichment analysis, 202 items were significantly enriched in BPs such as regulation of cell cycle phase transition and ribonucleotide metabolic process; 42 items were significantly enriched in CCs, such as mitochondrial inner membrane and cell cortex; 35 items were significantly enriched in MFs such as monoatomic ion channel activity and actin binding (Figure.2D, Table S7). CGs were also significantly enriched in 16 KEGG pathways, including fructose and mannose metabolism, tight junction, RNA

polymerase etc. (Figure.2E, Table S8). These pathways were mainly associated with metabolism and cell cycle, which suggested the function of CGs. A PPI network contained 51 core proteins and interactions such as GAPDH-LDOA and FLNA-FERMT2, was constructed (Figure.2F)

3.3 Prognostic model of 4 prognostic markers performed well

Univariate Cox model (P < 0.05) first screened out 16 genes passing the PH test (P > 0.05) (Figure.3A, B). When log(lambda.min) = -3.3572, SDF2L1, STK26, TDRKH and USP18 were identified as prognostic markers (Figure.3C, D; Table S9).

At the optimal cutoff of 0.02599047, TCGA-UCEC samples were partitioned into 177 high-risk and 206 low-risk patients (Table S10); applying a cutoff of -0.0145242 to the validation set yielded 77 high-risk and 86 low-risk patients (Table S11). Across both cohorts, risk scores corresponded closely to survival outcomes (Fig. 3E, F), and high-risk patients experienced markedly inferior prognosis relative to low-risk counterparts in both TCGA-UCEC (P < 0.0001) and the validation set (P < 0.001) (Fig. 3G, H). Prognostic model performed well in prediction of overall survival in 3, 5, 7 years in both TCGA-UCEC (AUC > 0.7) and validation set (AUC > 0.6) datasets (Fig. 3I, J) .

3.4 Stage and risk score were the independent prognostic factors

Tumor stage and risk score emerged as statistically significant risk factors in univariate Cox regression (P < 0.05) validated by a Proportional Hazards (PH) test (P > 0.05) (Fig. 4A, B); their independence as prognostic determinants was subsequently corroborated through multivariate Cox regression (P < 0.05) with a PH test (P > 0.05) (Fig. 4C, D). In nomogram, when the total points of the two factors was 168, the probability of death was 0.183, 0.264 and 0.314 in 3, 5, 7 years (Figure.4E). Calibration curves for the 3-, 5-, and 7-year time points tracked closely along the reference diagonal, indicating a high degree of concordance between model-predicted probabilities and actual outcomes (Fig. 4F). In the DCA curve, nomogram curve was higher than two extreme curves, suggesting good clinical efficacy of the model (Figure.4G). Further, nomogram also exhibited high accuracy in prediction with AUC > 0.7 in 3, 5, 7 years (Figure.4H).

3.5 Pathways and immune infiltration between high-risk and low-risk groups

The most prominent pathway differences between high- and low-risk groups involved ribosome biogenesis, cytokine-cytokine receptor interaction, and oxidative phosphorylation, collectively shedding light on molecular mechanisms underlying EC onset (Fig. 5A). Among the 28 immune cell types profiled across risk groups in the TCGA-UCEC cohort (Fig. 5B), 19 showed statistically significant differences,

including, activated CD4 T cells, activated dendritic cells and activated B cells (P < 0.05) (Fig. 5C, Table S12).

The strongest positive inter-cellular correlation was observed between macrophages and myeloid-derived suppressor cells (MDSC) (cor = 0.83, p < 0.001); conversely, type 2 T helper cells and CD56dim natural killer cells were the sole pair exhibiting a significant negative correlation (cor = -0.36, P < 0.05) (Fig. 5D). Regarding the associations between immune cells and prognostic markers, monocytes demonstrated the highest positive correlation with SDF2L1 (cor = 0.43, p < 0.001) and the steepest negative correlation with TDRKH (cor = -0.38, p < 0.001) (Fig. 5E, Table S13), suggesting that SDF2L1 may exert an antagonistic role relative to the other prognostic markers in modulating immune cell activity.

Exclusion (cor = 0.18, P = 0.00051) and dysfunction (cor = -0.51, P < 0.001) were associated with risk score while only the dysfunction was significantly lower in high-risk group (p < 0.0001), suggesting the potential dysfunction and exclusion tendency. TIDE had no correlation with risk score and difference in high-risk group, which indicated the slight probability of significant immunologic escape (Fig. 5F-H) .

3.6. Common pathways and drugs of prognostic markers

Specifically, there were pathways such as adherens junction enriched by SDF2L1, colorectal cancer enriched by STK26, basal transcription factors enriched by TDKH and DNA replication enriched by USP18 (Fig. 6A-D, Table S14-17). There were 12 common pathways shared by prognostic markers (Fig. 6E, Table S18), such as oxidative phosphorylation and cell cycle. Except cardiac muscle contraction, many pathways negatively enriched by SDF2L1, which was totally contrary to other prognostic markers (Fig. 6F) .

IC50 of 117 drugs, including AZD5991, GSK269962A etc., were notably different between high-risk and low-risk groups (Fig. 6G, Table S19). Risk scores were positively correlated to 35 drugs and negatively correlated to 8 drugs, such as UMI.77 showing the most significant correlation (Fig. 6H, Table S20). Drugs prediction results showed, 115 drugs were identified, including 7646-79-9 and ZINC commonly shared by prognostic markers, while there was no drugs predicted to target TDKH (Fig. 6I) .

4. Discussion

EC is a uterine malignancy arising from the epithelial lining[1], whose pathogenesis involves multiple contributing factors including obesity[5], abnormal lipid metabolism[6], and dysregulated chemokine signaling[47]. Triaptosis — an emerging mode of cell death driven by oxidative stress — has recently attracted attention for its potential involvement in EC progression[14]. This study utilized transcriptomic data from EC patients and integrated triaptosis-related genes to identify four key prognostic biomarkers (SDF2L1, STK26, TDRKH, USP18) through bioinformatic analysis. A prognostic risk model was established, through which the candidate biomarkers were found to potentially govern immune

microenvironmental remodeling, metabolic reprogramming, and susceptibility to targeted therapeutic interventions in EC.

SDF2L1 (Stromal cell-derived factor 2-like 1), a member of the stromal-derived factor family, is involved in endoplasmic reticulum (ER) stress, prevents the aggregation of misfolded proteins[48], and regulates metabolism. Its knockdown leads to increased glucose and triglyceride levels[49], while its expression inhibits cancer cell proliferation, migration, and invasion[50]. ER stress induces oxidative stress and autophagy[51], and SDF2L1 further participates in triaptosis through these processes[14]. ER stress-mediated apoptosis is an effective therapeutic approach for EC[52]; for example, the bioactive compound Wogonoside inhibits EC tumor growth and metastasis via ER stress[53]. Thus, targeting SDF2L1 to modulate ER stress may engage triaptosis and other cell death mechanisms, exerting anti-tumor effects. Additionally, impaired glucose metabolism accelerates EC progression promoted by dyslipidemia[54], indicating that SDF2L1's role in metabolic regulation may represent another avenue of involvement in EC. In summary, as a key regulator of ER stress, SDF2L1 may exert anti-tumor effects by suppressing misfolded protein aggregation and modulating glucose metabolism.

STK26 (Sterile 20-like kinase 26), classified as a serine/threonine protein kinase, phosphorylates downstream signaling molecules to drive processes including cell proliferation, epithelial-mesenchymal transition, cell death, and autophagy[55], while additionally governing immune cell polarization and inflammatory responses[55]. Overexpression of STK26 has been documented across multiple cancer types, where it sustains tumor cell survival through activation of autophagy-related signaling and concurrent suppression of apoptotic pathways[56], a profile consistent with unfavorable clinical outcomes. STK26 is also involved in oxidative stress, such as stabilizing ATF6 in the unfolded protein response induced by oxidative stress[57], as well as in immune inflammation. In summary, STK26 may be involved in regulating cell death processes such as phosphoinositide-mediated apoptosis through oxidative stress, and is associated with adverse clinical outcomes in EC.

TDRKH (Tudor and KH domain-containing) is a conserved mitochondrial Tudor domain protein expressed in immature oocytes, responsible for cleaving the 3' end of PIWI-interacting RNA (piRNA) during its maturation[58]. piRNA regulates meiotic and post-meiotic gene expression, suppresses harmful transposons to maintain DNA integrity, and promotes germ cell development[59, 60]. Reports on the biological function of TDRKH remain scarce; however, the significantly enriched pathways identified in this analysis point toward a putative regulatory role in cell cycle progression. Beyond this, mutations affecting DNA mismatch repair pathway genes represent an established etiological factor in EC, and aberrant upregulation of piRNA has been linked to enhanced tumor proliferation, migration, invasion, growth, and distant metastasis[61]. These studies suggest that TDRKH may contribute to EC progression by influencing piRNA function, and silencing TDRKH has been shown to inhibit EC proliferation and invasion[62]. In summary, TDRKH may influence malignant transformation in EC by maintaining genomic integrity and regulating the cell cycle. Studies indicate that aberrant piRNA upregulation is associated with EC proliferation and invasion, and silencing TDRKH inhibits these processes[2].

USP18 (Ubiquitin-specific protease 18) primarily removes ubiquitin or ubiquitin-like protein ISG15 from substrate proteins, positively regulating innate antiviral immunity[63]. Elevated ISG15 levels in EC promote G1/S phase transition and immune escape[64]. USP18 deletion triggers apoptosis and reduces cancer cell growth[65], while oxidative stress downregulates USP18 to induce inflammation and disrupt immune tolerance, promoting autoimmunity and cellular senescence[66], suggesting that USP18 may participate in triaptosis by responding to oxidative stress. Members of the USP18 family can maintain estrogen receptor α stability through deubiquitination activity, promoting adverse EC progression[67], indicating that USP18's deubiquitination activity may play a similar role. In summary, USP18's roles in immune response, oxidative stress, and cell death may be linked to EC progression.

This study's GSEA results identified a set of nine significantly enriched pathways differentiating the high- and low-risk endometrial carcinoma groups, most notably including ribosome and oxidative phosphorylation pathways[68, 69]. The enrichment of the ribosome pathway underscores its critical role in EC, where its biogenesis is essential for protein synthesis and cell growth, and its dysregulation is linked to oncogenesis[68, 70]; our key prognostic biomarkers align with this, as SDF2L1 may reduce ribosome numbers via ER stress[71], USP18 could modulate ribosomal activity through ISG15 conjugation[72], and TDRKH might influence it indirectly via piRNA processing[73]. Concurrently, the enrichment of oxidative phosphorylation highlights its relevance to EC progression[69], a process potentially regulated by SDF2L1 and STK26 through metabolic stress[51, 52], and interconnected with USP18-mediated deubiquitination of IGF2BP3 that promotes a glycolytic shift[74].

Immune infiltration profiling revealed markedly divergent immune landscapes between the two EC risk groups. Of note, monocyte and MDSC infiltration was substantially elevated in the high-risk group; both cell populations are well-established drivers of immunosuppressive signaling within the tumor microenvironment[75, 76]. In contrast, the low-risk group showed a higher infiltration level of Effector memory CD4 T cells, indicating a more active and favorable adaptive anti-tumor immune response. This differential immune landscape underscores the association between an immunosuppressive, pro-tumoral milieu and poor prognosis in EC.

The observed immune phenotype is intricately linked to the dysregulation of core cellular processes driven by the key prognostic biomarkers identified in this study—SDF2L1, USP18, and TDRKH. These biomarkers converge on perturbing ribosome biogenesis/function and oxidative phosphorylation[68, 69], which in turn reshape the immune microenvironment. For instance, SDF2L1, implicated in ER stress and oxidative stress regulation[51, 52, 77], may promote a milieu conducive to the recruitment and immunosuppressive function of MDSCs, whose activity relies on ROS and ER stress responses[78]. Similarly, the positive correlation between monocytes and SDF2L1, along with the negative correlation with TDRKH, suggests these biomarkers critically influence monocyte recruitment or polarization into pro-tumor macrophages, a process exacerbated under tumor conditions[79, 80]. Simultaneously, suppression of oxidative phosphorylation — likely attributable to the actions of these biomarkers — contributes to diminished anti-tumor immune responses, a finding consistent with the observed depletion of effector memory CD4 T cells in high-risk patients. Taken together, these results outline an

integrated mechanistic axis in which biomarker-induced perturbations in ribosomal function and metabolic reprogramming synergistically promote cancer cell expansion while cultivating an MDSC- and monocyte-enriched immunosuppressive niche, ultimately accelerating EC progression and conferring resistance to therapy[81, 82].

This study's drug prediction analysis, based on the common targeting of the key prognostic biomarkers SDF2L1, STK26, and USP18, identified two potential therapeutic agents: Cobalt chloride and zinc (ZINC).

The prediction of these agents aligns with known mechanisms relevant to cancer therapy. Cobalt chloride, a metal coordination compound, has been experimentally validated to suppress proliferation across multiple cancer cell types, trigger apoptotic pathways, and arrest the cell cycle, collectively reflecting its broad-spectrum anti-neoplastic activity[83]. Zinc, an essential trace element and cofactor for numerous metalloenzymes, is vital for cell membrane repair, proliferation, growth, and immune function[84]. Its role in cell death is highlighted by the ability of lysosomes to release zinc ions to trigger mitochondrial-mediated apoptosis[85]. Notably, zinc deficiency has been negatively correlated with EC risk, suggesting a protective effect[85]. Given the established roles of SDF2L1 and STK26 in oxidative stress and cell death pathways, and USP18 in deubiquitination and proliferation, cobalt chloride and zinc may exert therapeutic effects in EC by targeting these very mechanisms. Therefore, these computationally screened agents represent promising candidates for further investigation as they may influence EC progression by simultaneously targeting multiple prognostic biomarkers and regulating critical cell death processes.

5. Conclusions

This study utilized an integrated bioinformatics pipeline to identify four triaptosis-associated prognostic markers-SDF2L1, STK26, TDRKH, and USP18-in endometrial cancer, and constructed a prognostic model that reliably stratified patients. The risk score and tumor stage were confirmed as independent prognostic factors, and the derived nomogram exhibited robust predictive accuracy. Mechanistically, these markers appear to orchestrate endoplasmic reticulum stress, oxidative stress responses, immune microenvironment remodeling, and metabolic reprogramming, potentially converging on triaptosis-related cell death pathways. The observed enrichment of immunosuppressive cells in the high-risk group and the identification of common pathways and candidate drugs (e.g., cobalt chloride and zinc) further underscore the translational potential of these findings. Nevertheless, the work remains limited by its reliance on retrospective public datasets and computational predictions; functional experiments and prospective cohorts are necessary to validate the mechanistic links and clinical utility. Collectively, this study offers a novel triaptosis-centered prognostic framework for endometrial cancer and highlights avenues for mechanism-driven therapeutics.

Declarations

A**cknowledgments**

Authors' contributions

Nanqing Zhou: Conceptualization, Data curation, Validation, Visualization, Writing–original draft, Writing–review & editing. Jin Li: Data curation, Validation, Visualization, Writing–review & editing. XU Zhang: Validation, Writing–review & editing. Zirui Wu: Visualization, Writing–review & editing. Jie Ren: Conceptualization, Supervision, Writing–review & editing. Wenchi Xu: Conceptualization, Project administration, Supervision, Writing–review & editing. This work currently described has not been published, is not being considered for publication elsewhere, and its publication was approved by all authors.

Ethical approval and consent to participate

Not applicable.

Consent for publication

Not applicable.

Conflict of Interest

The authors declare that the research was conducted in the absence of any commercial or financial relationships that could be construed as a potential conflict of interest.

Availability of data and materials

All data analyzed in this study are publicly available. The TCGA-UCEC dataset was downloaded from The Cancer Genome Atlas (https://cancergenome.nih.gov/). Triaptosis-related genes were obtained from the published literature (Xie et al., 2025, reference[23]). TIDE scores were retrieved from http://tide.dfci.harvard.edu/.

Funding statement

Medical Research Union Found for High-quality health development of Guizhou Province 2024GZYXKYJJXM0113

References

1. Makker, V. et al. Endometrial cancer. *Nat. Rev. Dis. Primers*. **7** (1), 88. 10.1038/s41572-021-00324-8 (2021).
2. Wu, X. et al. Androgens in endometrial carcinoma: the killer or helper? *J. Endocrinol. Invest.* **46** (3), 457–464. 10.1007/s40618-022-01916-1 (2023).
3. Braun, M. M., Overbeek-Wager, E. A. & Grumbo, R. J. Diagnosis and Management of Endometrial Cancer. *Am. Fam Physician*. **93** (6), 468–474 (2016).

4. Klopp, A. H. et al. Omental adipose tissue-derived stromal cells promote vascularization and growth of endometrial tumors. *Clin. Cancer Res.* **18** (3), 771–782. 10.1158/1078-0432.Ccr-11-1916 (2012).
5. Onstad, M. A., Schmandt, R. E. & Lu, K. H. Addressing the Role of Obesity in Endometrial Cancer Risk, Prevention, and Treatment. *J. Clin. Oncol.* **34** (35), 4225–4230. 10.1200/jco.2016.69.4638 (2016).
6. Wang, X., Li, Y., Hou, X., Li, J. & Ma, X. Lipid metabolism reprogramming in endometrial cancer: biological functions and therapeutic implications. *Cell. Commun. Signal.* **22** (1), 436. 10.1186/s12964-024-01792-7 (2024).
7. Sobstyl, M., Brecht, P., Sobstyl, A., Mertowska, P. & Grywalska, E. The Role of Microbiota in the Immunopathogenesis of Endometrial Cancer. *Int. J. Mol. Sci.* **23** (10). 10.3390/ijms23105756 (2022).
8. Muhleisen, A. L. & Herbst-Kralovetz, M. M. Menopause and the vaginal microbiome. *Maturitas* **91**, 42–50. 10.1016/j.maturitas.2016.05.015 (2016).
9. Caselli, E. et al. Atopobium vaginae And Porphyromonas somerae Induce Proinflammatory Cytokines Expression In Endometrial Cells: A Possible Implication For Endometrial Cancer? *Cancer Manag Res.* **11**, 8571–8575. 10.2147/cmar.S217362 (2019).
10. Modugno, F., Ness, R. B., Chen, C. & Weiss, N. S. Inflammation and endometrial cancer: a hypothesis. *Cancer Epidemiol. Biomarkers Prev.* **14** (12), 2840–2847. 10.1158/1055-9965.Epi-05-0493 (2005).
11. Yu, M. et al. N-glycosylation of uterine endometrium determines its receptivity. *J. Cell. Physiol.* **235** (2), 1076–1089. 10.1002/jcp.29022 (2020).
12. Zhang, L. et al. The Sweet Relationship between the Endometrium and Protein Glycosylation. *Biomolecules* **14** (7). 10.3390/biom14070770 (2024).
13. Galant, N. et al. Molecular Classification of Endometrial Cancer and Its Impact on Therapy Selection. *Int. J. Mol. Sci.* **25** (11). 10.3390/ijms25115893 (2024).
14. Swamynathan, M. M. et al. Dietary pro-oxidant therapy by a vitamin K precursor targets PI 3-kinase VPS34 function. *Science* **386** (6720), eadk9167. 10.1126/science.adk9167 (2024).
15. Jia, M. et al. ULK1-mediated metabolic reprogramming regulates Vps34 lipid kinase activity by its lactylation. *Sci. Adv.* **9** (22), eadg4993. 10.1126/sciadv.adg4993 (2023).
16. Qi, C. et al. Vps34 Inhibits Hepatocellular Carcinoma Invasion by Regulating Endosome-Lysosome Trafficking via Rab7-RILP and Rab11. *Cancer Res. Treat.* **54** (1), 182–198. 10.4143/crt.2020.578 (2022).
17. Harada, T. et al. Apoptosis in human endometrium and endometriosis. *Hum. Reprod. Update*. **10** (1), 29–38. 10.1093/humupd/dmh007 (2004).
18. Avagliano, L. et al. Autophagy in Normal and Abnormal Early Human Pregnancies. *Reprod. Sci.* **22** (7), 838–844. 10.1177/1933719114565036 (2015).
19. Su, P. et al. ERRα promotes glycolytic metabolism and targets the NLRP3/caspase-1/GSDMD pathway to regulate pyroptosis in endometrial cancer. *J. Exp. Clin. Cancer Res.* **42** (1), 274. 10.1186/s13046-023-02834-7 (2023).

20. Ma, F. F. et al. miRNA omics reveal neferine induces apoptosis through Ca(2+)mediated endoplasmic reticulum stress pathway in human endometrial cancer. *Phytomedicine* **134**, 155988. 10.1016/j.phymed.2024.155988 (2024).
21. Rai, R., Dey, D. K., Benbrook, D. M. & Chandra, V. Niclosamide causes lysosome-dependent cell death in endometrial cancer cells and tumors. *Biomed. Pharmacother*. **161**, 114422. 10.1016/j.biopha.2023.114422 (2023).
22. Huang, Y., Li, R. & Yang, Y. Role of Pyroptosis in Gynecological Oncology and Its Therapeutic Regulation. *Biomolecules* **12** (7). 10.3390/biom12070924 (2022).
23. Xie, J., Zhang, M. & Qi, M. Integrating Machine Learning Algorithms to Construct a Triaptosis-Related Prognostic Model in Melanoma. *Cancer Manag Res.* **17**, 1127–1141. 10.2147/cmar.S525738 (2025).
24. Hänzelmann, S., Castelo, R. & Guinney, J. GSVA: gene set variation analysis for microarray and RNA-seq data. *BMC Bioinform.* ;**14**:7. doi:10.1186/1471-2105-14-7 (2013).
25. Gustavsson, E. K., Zhang, D., Reynolds, R. H., Garcia-Ruiz, S. & Ryten, M. ggtranscript: an R package for the visualization and interpretation of transcript isoforms using ggplot2. *Bioinformatics* **38** (15), 3844–3846. 10.1093/bioinformatics/btac409 (2022).
26. Langfelder, P. & Horvath, S. WGCNA: an R package for weighted correlation network analysis. *BMC Bioinform.* **9**, 559. 10.1186/1471-2105-9-559 (2008).
27. Love, M. I., Huber, W. & Anders, S. Moderated estimation of fold change and dispersion for RNA-seq data with DESeq2. *Genome Biol.* **15** (12), 550. 10.1186/s13059-014-0550-8 (2014).
28. Gu, Z. Complex heatmap visualization. *Imeta* **1** (3), e43. 10.1002/imt2.43 (2022).
29. Chen, H. & Boutros, P. C. VennDiagram: a package for the generation of highly-customizable Venn and Euler diagrams in R. *BMC Bioinform.* **12**, 35. 10.1186/1471-2105-12-35 (2011).
30. Yu, G., Wang, L. G., Han, Y. & He, Q. Y. clusterProfiler: an R package for comparing biological themes among gene clusters. *Omics* **16** (5), 284–287. 10.1089/omi.2011.0118 (2012).
31. Voss, J. S. et al. Changes in specimen preparation method may impact urine cytologic evaluation. *Am. J. Clin. Pathol.* **130** (3), 428–433. 10.1309/vp1xq5gpq687w1hu (2008).
32. Li-Fei, M. et al. Risk scoring model for lung adenocarcinoma based on PD-L1 related signature reveals prognostic predictability and correlation with tumor immune microenvironment genes was constructed. *Front. Immunol.* **16**, 1601982. 10.3389/fimmu.2025.1601982 (2025).
33. Milne, C. P. & Kaitin, K. I. Translational medicine: an engine of change for bringing new technology to community health. *Sci. Transl Med.* **1** (5), 5cm. 10.1126/scitranslmed.3000222 (2009).
34. Yu, J., Zhao, B. & Yu, Y. Identification and Validation of Cytotoxicity-Related Features to Predict Prognostic and Immunotherapy Response in Patients with Clear Cell Renal Cell Carcinoma. *Genet. Res. (Camb)*. **2024**, 3468209. 10.1155/2024/3468209 (2024).
35. Sachs, M. C. & plotROC A Tool for Plotting ROC Curves. *J. Stat. Softw.* 79. 10.18637/jss.v079.c02 (2017).

36. Zhu, H. et al. Insights into a Machine Learning-Based Palmitoylation-Related Gene Model for Predicting the Prognosis and Treatment Response of Breast Cancer Patients. *Technol. Cancer Res. Treat.* **23**, 15330338241263434. 10.1177/15330338241263434 (2024).
37. Liberzon, A. et al. The Molecular Signatures Database (MSigDB) hallmark gene set collection. *Cell. Syst.* **1** (6), 417–425. 10.1016/j.cels.2015.12.004 (2015).
38. Qi, W. Y. et al. Immune cells in metabolic associated fatty liver disease: Global trends and hotspots (2004–2024). *World J. Hepatol.* **17** (3), 103327. 10.4254/wjh.v17.i3.103327 (2025).
39. Zhou, W. et al. Identification and mechanism analysis of biomarkers related to butyrate metabolism in COVID-19 patients. *Ann. Med.* **57** (1), 2477301. 10.1080/07853890.2025.2477301 (2025).
40. Zhao, P., Zhen, H., Zhao, H., Huang, Y. & Cao, B. Identification of hub genes and potential molecular mechanisms related to radiotherapy sensitivity in rectal cancer based on multiple datasets. *J. Transl Med.* **21** (1), 176. 10.1186/s12967-023-04029-2 (2023).
41. Robin, X. et al. pROC: an open-source package for R and S + to analyze and compare ROC curves. *BMC Bioinform.* **12**, 77. 10.1186/1471-2105-12-77 (2011).
42. Snyder, R. A. A. & Good Mother *Jama* ;**325**(18):1837–1838. doi:10.1001/jama.2021.6271 (2021).
43. Wang, J. et al. PROS1 shapes the immune-suppressive tumor microenvironment and predicts poor prognosis in glioma. *Front. Immunol.* **13**, 1052692. 10.3389/fimmu.2022.1052692 (2022).
44. Yoo, M. et al. DSigDB: drug signatures database for gene set analysis. *Bioinformatics* **31** (18), 3069–3071. 10.1093/bioinformatics/btv313 (2015).
45. Kuleshov, M. V. et al. Enrichr: a comprehensive gene set enrichment analysis web server 2016 update. *Nucleic Acids Res.* **44** (W1), W90–W97. 10.1093/nar/gkw377 (2016).
46. Shannon, P. et al. Cytoscape: a software environment for integrated models of biomolecular interaction networks. *Genome Res.* **13** (11), 2498–2504. 10.1101/gr.1239303 (2003).
47. Liu, P., Long, P., Huang, Y., Sun, F. & Wang, Z. CXCL12/CXCR4 axis induces proliferation and invasion in human endometrial cancer. *Am. J. Transl Res.* **8** (4), 1719–1729 (2016).
48. Luo, C., Zhang, Z., Su, Q. & Mo, W. Identification of Phosphorylated Proteins Regulated by SDF2L1 in Nasopharyngeal Carcinoma Cells. *Evol. Bioinform Online*. **18**, 11769343221095862. 10.1177/11769343221095862 (2022).
49. Sasako, T. et al. Hepatic Sdf2l1 controls feeding-induced ER stress and regulates metabolism. *Nat. Commun.* **10** (1), 947. 10.1038/s41467-019-08591-6 (2019).
50. Zhang, L. et al. SDF2L1 Inhibits Cell Proliferation, Migration, and Invasion in Nasopharyngeal Carcinoma. *Biomed. Res. Int.* **2020**, 1970936. 10.1155/2020/1970936 (2020).
51. Lin, Y., Jiang, M., Chen, W., Zhao, T. & Wei, Y. Cancer and ER stress: Mutual crosstalk between autophagy, oxidative stress and inflammatory response. *Biomed. Pharmacother*. **118**, 109249. 10.1016/j.biopha.2019.109249 (2019).
52. Zhou, X. et al. Natural products modulate cell apoptosis: a promising way for treating endometrial cancer. *Front. Pharmacol.* **14**, 1209412. 10.3389/fphar.2023.1209412 (2023).

53. Chen, S. et al. Wogonoside inhibits tumor growth and metastasis in endometrial cancer via ER stress-Hippo signaling axis. *Acta Biochim. Biophys. Sin (Shanghai)*. **51** (11), 1096–1105. 10.1093/abbs/gmz109 (2019).
54. Zhou, J. et al. Metabolic disorders sensitise endometrial carcinoma through endoplasmic reticulum stress. *Cell. Mol. Biol. Lett.* **27** (1), 110. 10.1186/s11658-022-00412-x (2022).
55. Getu, A. A., Zhou, M., Cheng, S. Y. & Tan, M. The mammalian Sterile 20-like kinase 4 (MST4) signaling in tumor progression: Implications for therapy. *Cancer Lett.* **563**, 216183. 10.1016/j.canlet.2023.216183 (2023).
56. Li, K. et al. Targeting STK26 and ATG4B: miR-22-3p as a modulator of autophagy and tumor progression in HCC. *Transl Oncol.* **51**, 102214. 10.1016/j.tranon.2024.102214 (2025).
57. Ding, Y. et al. STK26 Promotes the Stabilization of ATF6 to Facilitate the Progression of Colorectal Cancer. *Int. J. Mol. Sci.* **26** (16). 10.3390/ijms26168052 (2025).
58. Virant-Klun, I., Leicht, S., Hughes, C. & Krijgsveld, J. Identification of Maturation-Specific Proteins by Single-Cell Proteomics of Human Oocytes. *Mol. Cell. Proteom.* **15** (8), 2616–2627. 10.1074/mcp.M115.056887 (2016).
59. Ding, D. et al. Mitochondrial membrane-based initial separation of MIWI and MILI functions during pachytene piRNA biogenesis. *Nucleic Acids Res.* **47** (5), 2594–2608. 10.1093/nar/gky1281 (2019).
60. Tan, M. et al. PIWIL3 Forms a Complex with TDRKH in Mammalian Oocytes. *Cells* **9** (6). 10.3390/cells9061356 (2020).
61. Silvia, B. J. et al. A comprehensive review on the role of PIWI-interacting RNA (piRNA) in gynecological cancers. *Life Sci.* **357**, 123065. 10.1016/j.lfs.2024.123065 (2024).
62. Wang, B. & Ma, X. Three RNA-binding protein signature as a novel biomarker to predict endometrial cancer prognosis. *Am. J. Transl Res.* **15** (1), 476–492 (2023).
63. Hou, J. et al. USP18 positively regulates innate antiviral immunity by promoting K63-linked polyubiquitination of MAVS. *Nat. Commun.* **12** (1), 2970. 10.1038/s41467-021-23219-4 (2021).
64. Zhao, X. et al. Interferon–stimulated gene 15 promotes progression of endometrial carcinoma and weakens antitumor immune response. *Oncol. Rep.* **47** (6). 10.3892/or.2022.8321 (2022).
65. Mustachio, L. M. et al. Evidence for the ISG15-Specific Deubiquitinase USP18 as an Antineoplastic Target. *Cancer Res.* **78** (3), 587–592. 10.1158/0008-5472.Can-17-1752 (2018).
66. Lee, E. J. et al. ISG15-USP18 Dysregulation by Oxidative Stress Promotes IFN-γ Secretion from CD8 + T Cells in Vitiligo. *J. Invest. Dermatol.* **144** (2), 273–83e11. 10.1016/j.jid.2023.08.006 (2024).
67. Su, Y. et al. Ubiquitin-specific peptidase 14 maintains estrogen receptor α stability via its deubiquitination activity in endometrial cancer. *J. Biol. Chem.* **299** (1), 102734. 10.1016/j.jbc.2022.102734 (2023).
68. Elhamamsy, A. R., Metge, B. J., Alsheikh, H. A., Shevde, L. A. & Samant, R. S. Ribosome Biogenesis: A Central Player in Cancer Metastasis and Therapeutic Resistance. *Cancer Res.* **82** (13), 2344–2353. 10.1158/0008-5472.Can-21-4087 (2022).

69. Nolfi-Donegan, D., Braganza, A. & Shiva, S. Mitochondrial electron transport chain: Oxidative phosphorylation, oxidant production, and methods of measurement. *Redox Biol.* **37**, 101674. 10.1016/j.redox.2020.101674 (2020).
70. Bianco, C. & Mohr, I. Ribosome biogenesis restricts innate immune responses to virus infection and DNA. *Elife* 8. 10.7554/eLife.49551 (2019).
71. Li, H. et al. Quantitative proteomics reveals the mechanism of endoplasmic reticulum stress-mediated pulmonary fibrosis in mice. *Heliyon* **10** (20), e39150. 10.1016/j.heliyon.2024.e39150 (2024).
72. Held, T., Basler, M., Knobeloch, K. P. & Groettrup, M. Evidence for an involvement of the ubiquitin-like modifier ISG15 in MHC class I antigen presentation. *Eur. J. Immunol.* **51** (1), 138–150. 10.1002/eji.202048646 (2021).
73. Sun, Y. H. et al. Ribosomes guide pachytene piRNA formation on long intergenic piRNA precursors. *Nat. Cell. Biol.* **22** (2), 200–212. 10.1038/s41556-019-0457-4 (2020).
74. Wang, B. et al. LIN28B induced PCAT5 promotes endometrial cancer progression and glycolysis via IGF2BP3 deubiquitination. *Cell. Death Dis.* **15** (4), 242. 10.1038/s41419-024-06564-2 (2024).
75. Hegde, S., Leader, A. M. & Merad, M. MDSC: Markers, development, states, and unaddressed complexity. *Immunity* **54** (5), 875–884. 10.1016/j.immuni.2021.04.004 (2021).
76. Gabrilovich, D. I. Myeloid-Derived Suppressor Cells. *Cancer Immunol. Res.* **5** (1), 3–8. 10.1158/2326-6066.Cir-16-0297 (2017).
77. (!!! INVALID CITATION !!! [71]).
78. Bronte, V. et al. Recommendations for myeloid-derived suppressor cell nomenclature and characterization standards. *Nat. Commun.* **7**, 12150. 10.1038/ncomms12150 (2016).
79. Xiao, L., He, Y., Peng, F., Yang, J. & Yuan, C. Endometrial Cancer Cells Promote M2-Like Macrophage Polarization by Delivering Exosomal miRNA-21 under Hypoxia Condition. *J. Immunol. Res.* **2020**, 9731049. 10.1155/2020/9731049 (2020).
80. Machida, H. et al. Significance of Monocyte Counts at Recurrence on Survival Outcome of Women With Endometrial Cancer. *Int. J. Gynecol. Cancer*. **27** (2), 302–310. 10.1097/igc.0000000000000865 (2017).
81. Yokoi, E. et al. The role of myeloid-derived suppressor cells in endometrial cancer displaying systemic inflammatory response: clinical and preclinical investigations. *Oncoimmunology* **8** (12), e1662708. 10.1080/2162402x.2019.1662708 (2019).
82. Mabuchi, S. & Sasano, T. Myeloid-Derived Suppressor Cells as Therapeutic Targets in Uterine Cervical and Endometrial Cancers. *Cells* **10** (5). 10.3390/cells10051073 (2021).
83. Mahey, S. et al. Effect of cobalt(II) chloride hexahydrate on some human cancer cell lines. *Springerplus* **5** (1), 930. 10.1186/s40064-016-2405-0 (2016).
84. Lin, P. H. et al. Zinc in Wound Healing Modulation. *Nutrients* **10** (1). 10.3390/nu10010016 (2017).

85. Du, W. et al. Lysosomal Zn(2+) release triggers rapid, mitochondria-mediated, non-apoptotic cell death in metastatic melanoma. *Cell. Rep.* **37** (3), 109848. 10.1016/j.celrep.2021.109848 (2021).

Figures

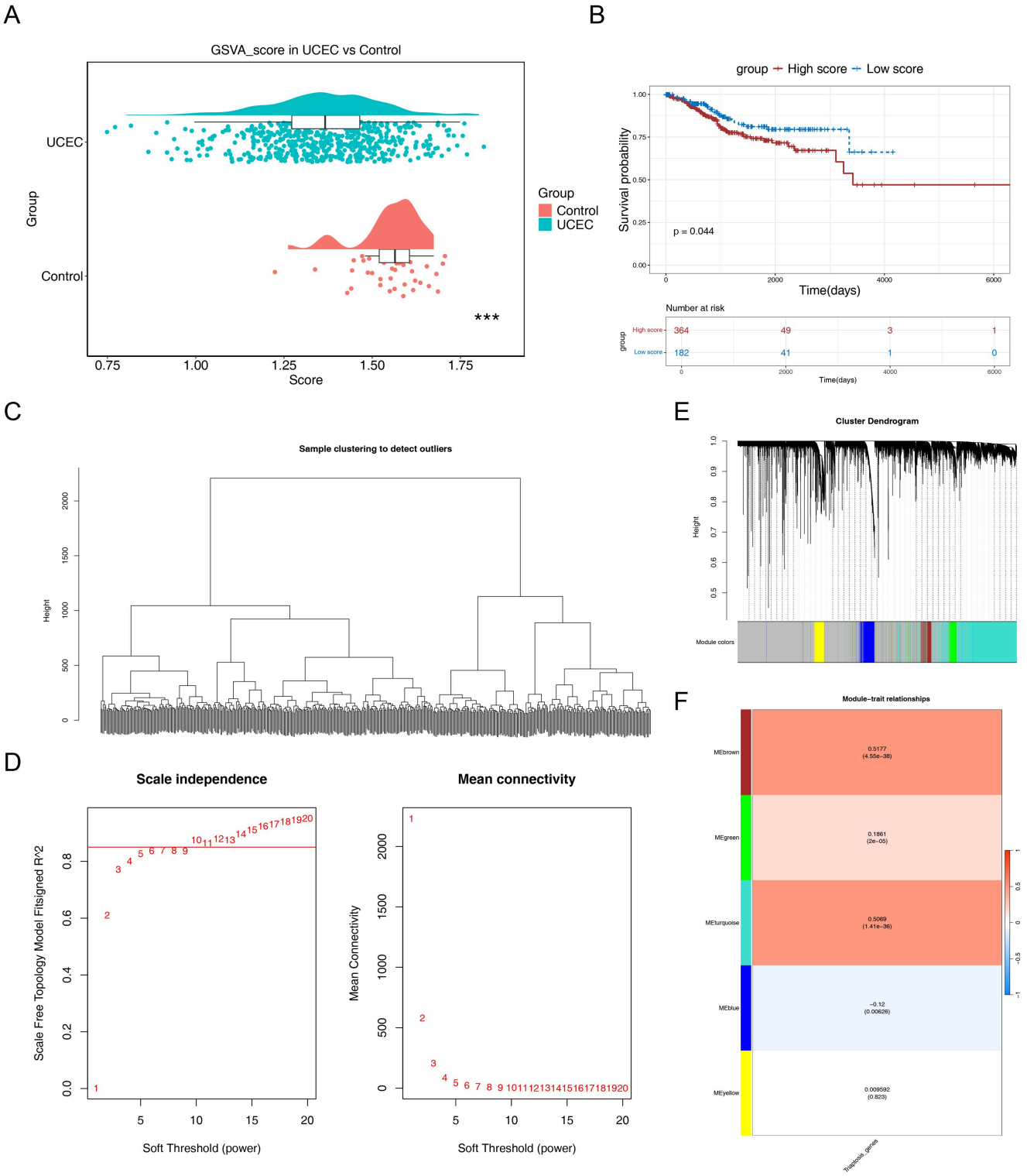


Figure 1

Acquisition of WGCNA-TRGs. (A) TRGs scores between EC and control groups, *** represents P < 0.001. (B) Kaplan-Meier (K-M) curve, showing the survival state and time. (C) Sample clustering in GSE57338, cutHeight = 100. (D) Scale independence model and mean connectivity of power, R2 > 0.85 and mean connectivity < 200. (E) Cluster dendrogram, minModuleSize = 100. (F) 5 modules with minModuleSize = 100 and mergeCutHeight = 0.3, key modules with cor > 0.3 and P < 0.05.

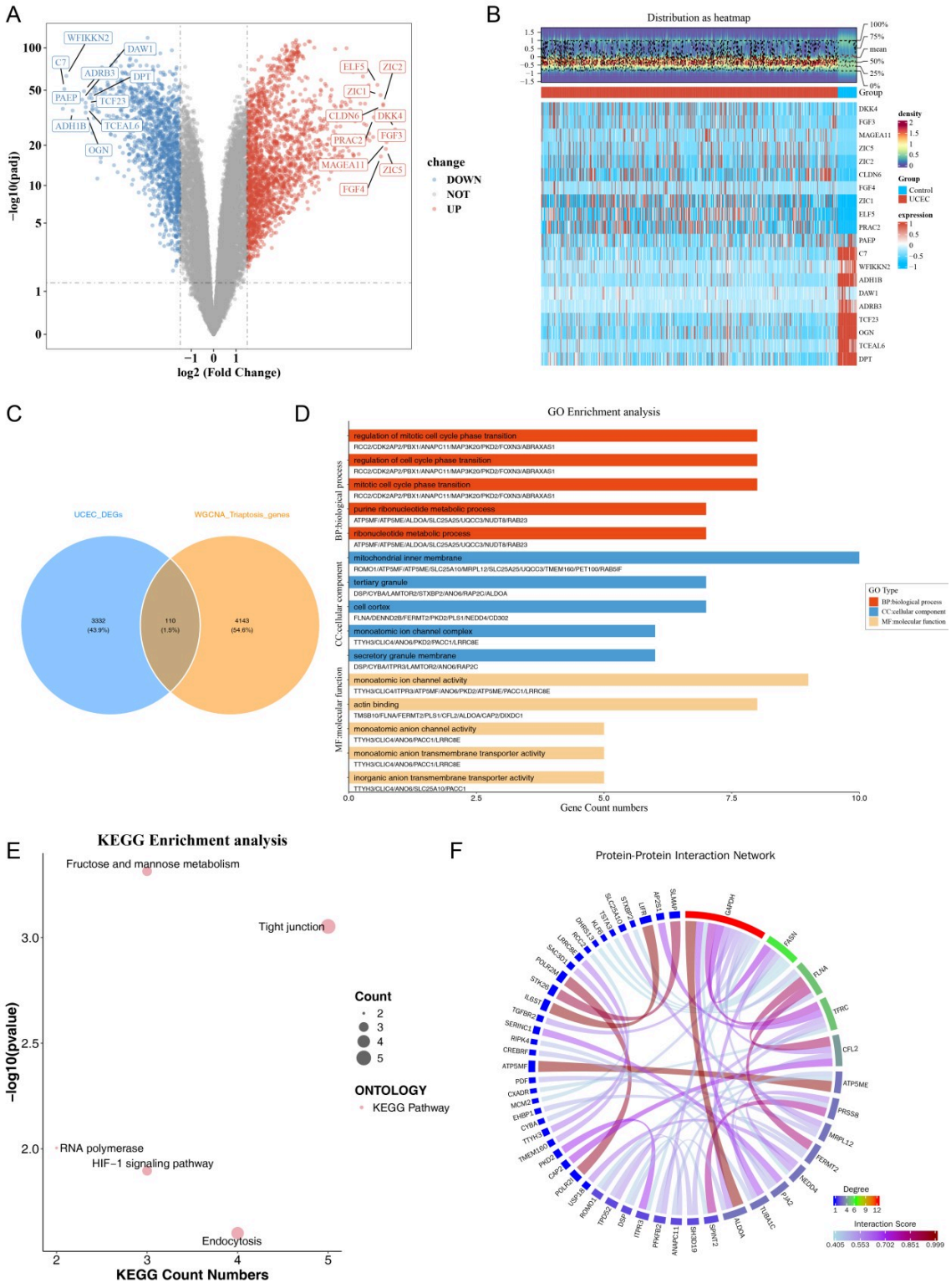


Figure 2

Acquisition of candidate genes (CGs) . (A) Volcano plot and (B) Heatmap of differentially expressed genes in EC. (C) Venn diagram of genes related to Triaptosis and DEGs in TCGA-UCEC, showing their intersecting genes as CGs. (D) GO pathways and (E) KEGG pathways enriched by CGs. (F) PPI network of CGs, different nodes represent distinct proteins and lines represent the potential interaction among each genes.

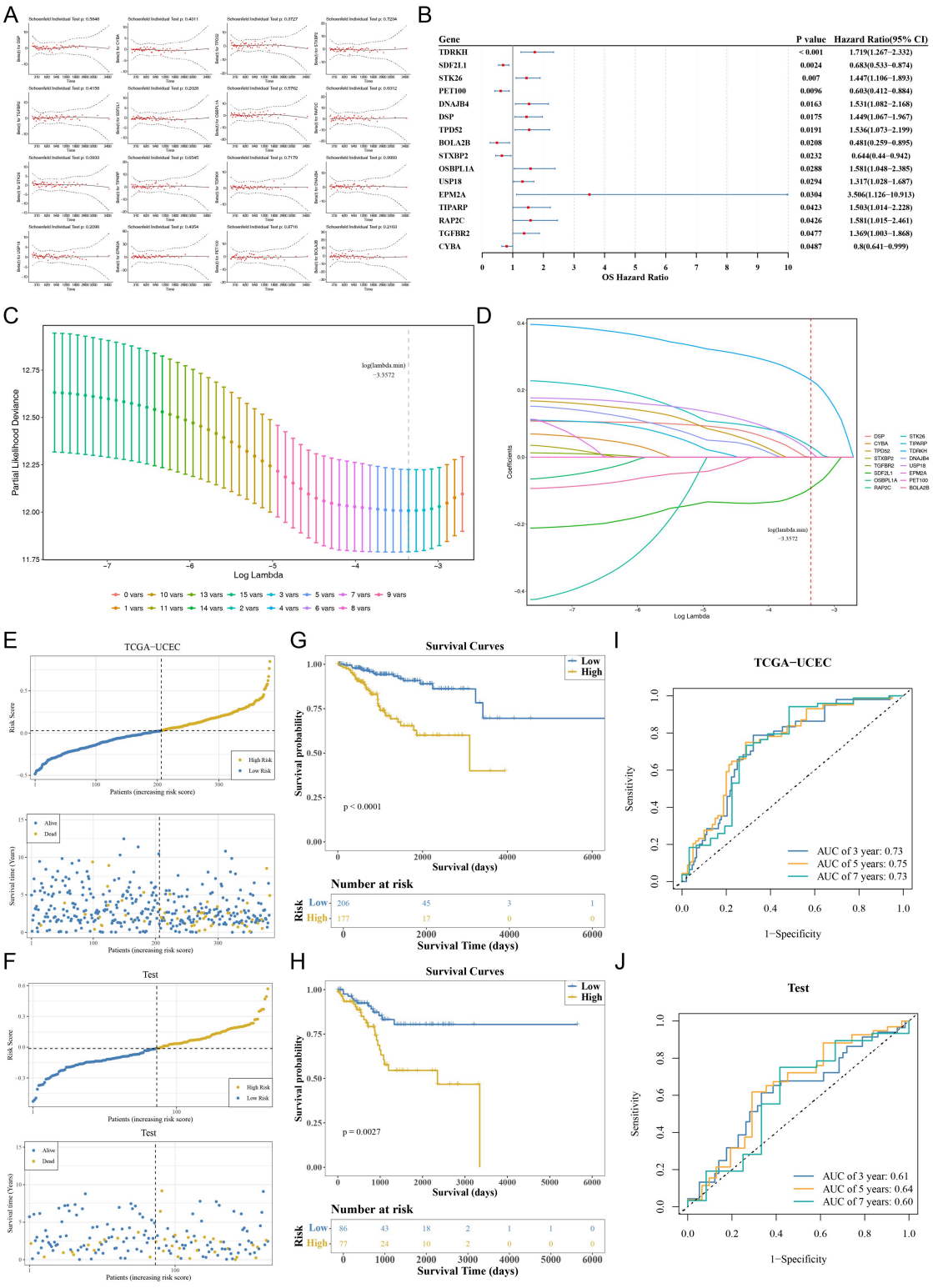


Figure 3

Determination of prognostic markers. (A) PH test of candidate prognostic markers. (B) Forest plot of univariate Cox model. (C) Lambda selection plot, the horizontal axis symbolizes log (Lambda) values and the vertical axis symbolizes regression cross-validation errors. (D) Coefficient Path Plot, showing prognostic markers with coefficient ≠ 0, when lambda.min = 0.0087. Risk score and survival time of patients in (E) TCGA-UCEC and (F) validation set. Survival probability between high-risk and low-risk groups in (G) TCGA-UCEC and (H) validation set. ROC curve of the survival rate in 3, 5, 7 years of (I) TCGA-UCEC and (J) validation set.

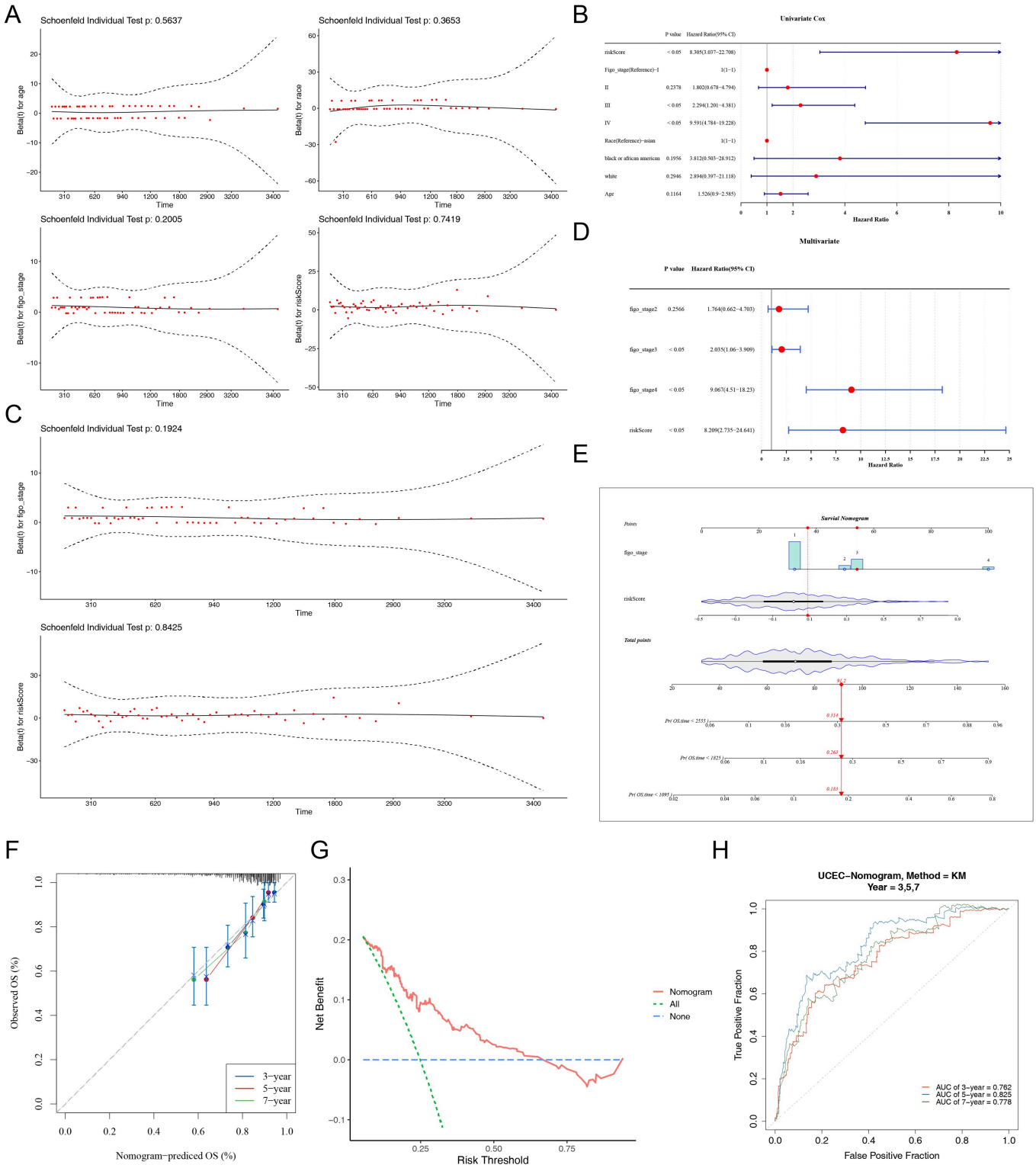


Figure 4

Stage and risk score were the independent prognostic factors. (A) PH test and (B) forest plot of univariate Cox analysis. (C) PH test and (D) forest plot of multivariate Cox analysis. (E) Nomogram of prognostic factors, where "Point" represents individual scores on the scale; "Total Point" represents the combined score of the prognostic factors, "Pr" represents the probability of EC death. (F) Calibration between the actual curve and predicted curve of nomogram. (G) DCA curves of the nomogram, demonstrating good clinical efficacy. (H) ROC curves of the nomogram, demonstrating good predictive performance.

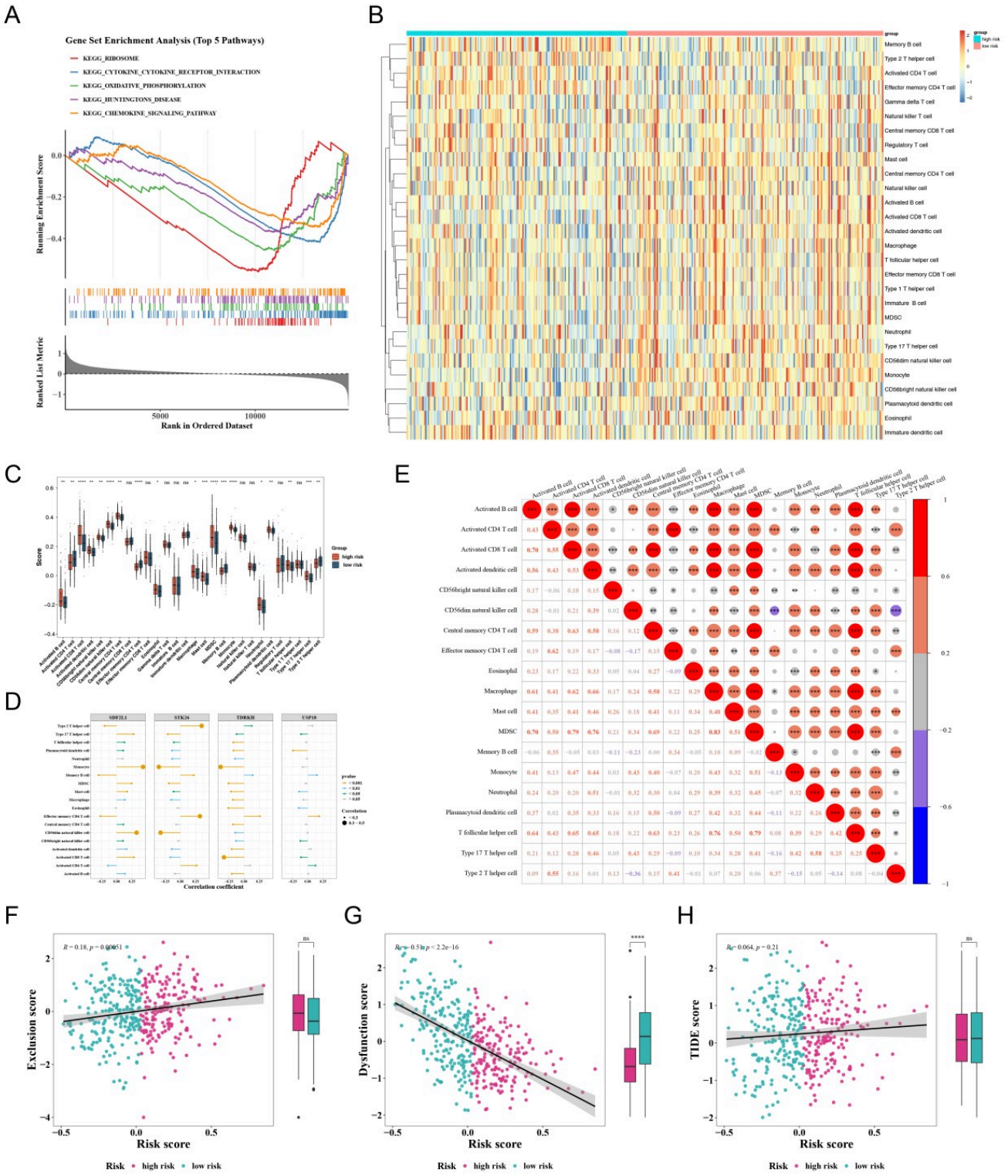


Figure 5

Pathways and immune infiltration between high-risk and low-risk groups. (A) The significantly different pathways between high-risk and low-risk groups. (B) The proportions of 28 immune cells. (C) Different immune cells between high-risk and low-risk groups. (D) Correlation among immune cells. (E) Correlation between immune cells and prognostic markers. (F-H) Correlation of risk score with exclusion,

dysfunction and TIDE, and their differences between high-risk and low-risk groups. * represents the significant level, * P < 0.05, ** p < 0.01, *** p < 0.001, ns represents no significant difference.

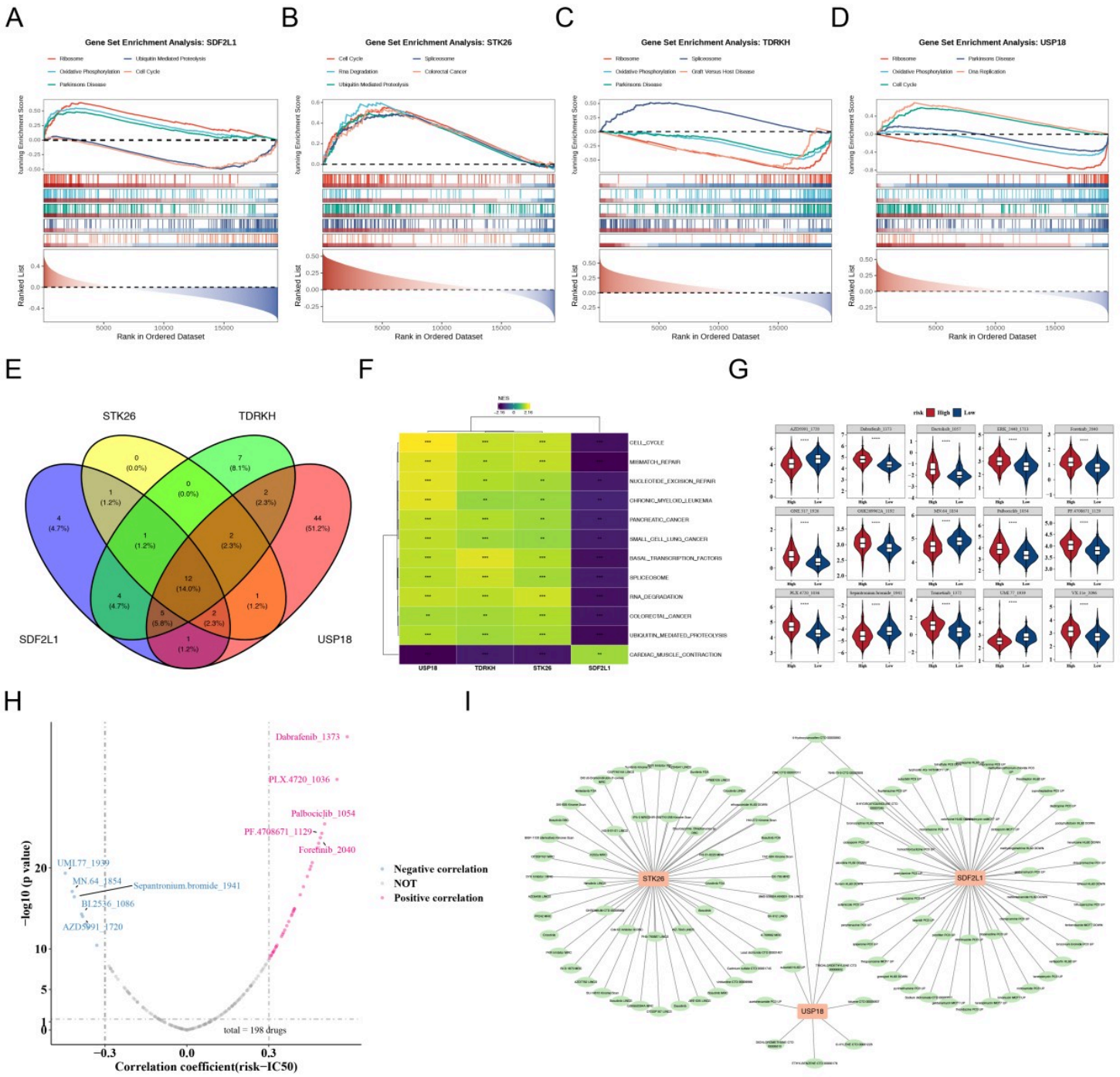


Figure 6

Common pathways and drugs of prognostic markers. Top5 pathways enriched by (A) SDF2L1, (B) STK26, (C) TDKH and (D) USP18. (E) Venn plot of common pathways shared by prognostic markers. (F) NES heatmap of common pathways, purple represent negative enriched, yellow represent positive enriched. (G) Drug sensitivity between high-risk and low-risk groups. (H) Correlation between IC50 and

risk scores, red represents positive-related, blue represents negative-related. (I) potential drugs targeting prognostic markers. * represents the significant level, * P < 0.05, ** p < 0.01, *** p < 0.001.

Supplementary Files

This is a list of supplementary files associated with this preprint. Click to download.

- TableS9.csv
- TableS12.csv
- TableS3.csv
- TableS8.csv
- TableS13.csv
- TableS1.xlsx
- TableS18.csv
- TableS2.csv
- TableS16.csv
- TableS14.csv
- file.docx
- TableS6.csv
- TableS19.csv
- TableS20.csv
- TableS11.csv
- TableS17.csv
- TableS15.csv
- TableS4.csv
- TableS7.csv
- TableS10.csv
- TableS5.csv
- Supplementarymaterial.pdf